International Journal of Steel Structures (2019) 19(3):733–746
https://doi.org/10.1007/s13296-018-0158-z

Online ISSN 2093-6311
Print ISSN 1598-2351

Experimental Study of the Mechanical Performance of Corrugated Steel Plate-Concrete Composite Structures

Baodong Liu[1] · Zhenan Zhang[2] · Minqiang Zhang[3] · Xiaoxi Wang[1]

Received: 9 October 2017 / Accepted: 27 August 2018 / Published online: 3 September 2018

Abstract

This paper presents a comparative study on the composite structure of Corrugated Steel Plate (CSP) with normal and rubberized concrete. One CSP-normal-concrete plate and two CSP arch structures composited with different concretes are established. A theoretical section-property deduction is derived, which demonstrated that the flexural rigidity of such composite structure increased notably. Static and dynamic mechanical experiments are also conducted. Experimental results agree with expectations, and the measured results on plate structures verified the effectiveness of the analytical and numerical solutions. Comparing the deflection of two composite arches shows that the rubberized concrete composite arch has smaller flexural and compressive stiffnesses, resulting in larger deflection. The rubberized concrete composite arch has higher steel stress, lower concrete stress and better energy-dissipating capacity compared with the normal concrete composite arch. Therefore, the CSP-rubberized concrete composite structure is more suitable for anti-shock and earthquake-resistant structures.

Keywords Composite structure · Corrugated-steel plate · Rubberized concrete · Experimental study · Mechanical performance

List of symbols

I'	The total moment of inertia
A'	The total area
α_e	The modulus ratio of steel and concrete
A_c	Primary concrete area
A'_c	Converted equivalent steel area
b	Wave pitch of the CSP
b_{eq}	Length of equivalent steel materials transformed by former concrete
T	Width of concrete covering
t	Plate thickness of CSP
h	Wave depth of CSP
y_c	The centroid of the concrete
y_{cp}	The centroid of the composite section
E_s	Modulus of steel
E_c	Modulus of concrete
A_s	Area of steel
I_s	CSP's moment of inertia
δ	Vertical deflection
σ_{spt}	Steel normal stress
M	Bending moment under external load
M'	Bending moment of micro-segment ds under unit load
E_sI'	The flexural rigidity
y'	The distance between the centroid and the corrugation valley
y	The distance between the centroid and top of concrete
σ_{cpt}	Concrete stress
α_{el}	Ratio between modulus of steel and normal concrete
E_{cpt}	Modulus of normal concrete

✉ Baodong Liu
baodongliu@vip.sina.com

Zhenan Zhang
zzn@bmedi.cn

Minqiang Zhang
zhangminqiangccecc@outlook.com

Xiaoxi Wang
wxxsunny@yeah.net

[1] School of Civil Engineering, Beijing Jiaotong University, Beijing, China

[2] Beijing General Municipal Engineering Design & Research Institute Co., Ltd, Beijing, China

[3] China Civil Engineering Construction Corporation, Beijing, China

1 Introduction

Corrugated Steel Plate (CSP) is an orthotropic plate material, which is universally applied in culvert structures, dispersing the upper load by soil-structure interaction between corrugated steel structures and surrounding soils (Beben 2014). Nevertheless, when the span rises or the covered soil thickens, these culverts are prone to be destroyed (Choi et al. 2009).

There are many measures to strengthen CSP, such as "CSP + CSP" or "CSP reinforced with concrete Concrete-Filled Steel Tubes (CFSTs)" (Machelski et al. 2013). Earlier applications of CSP-concrete structures were concentrated on three-dimensional concrete-lined CSP shelter structures in military fields (Liu 2001). These concrete-lined CSP structures have higher strength and stiffness to avoid collapse. Another composite measure involved inverting one CSP into another, pouring concrete inside the gap with a screwed bolt between the two CSPs, which has been optimized to achieve its ultimate bearing capacity and bending stiffness (Morrison 2005; Flener 2009). Vinoth Kumar and Kavitha (2016) studied 650-mm-wide, 100-mm-high, 1250-mm-long concrete sandwich panels. The test results showed the concrete weight in the panel had been reduced by 17%. A sandwich panel is more elastic, and its load-carrying capacity is 1.5 times greater than that of a reinforced concrete panel. No cracks were found in the compression zone of the panel. Furthermore, Yu et al. (2012) produced a calculation method for reinforced concrete shell with CSP lining. The deflection of reinforced concrete shell with (or without) CSP lining was compared, concluding that CSP has a notable effect on restricted structural deflection. With regard to the application of culvert in buried underground structure, Kang and Davidson (2013) evaluated the structural effects of the concrete lining in concrete-lined corrugated steel pipes (CLCSP) and proposed a design methodology. In other research, the performance limits of concrete-encased pipes were identified and design procedures were described. The encasement holds the flexible pipe in its circular shape and supports most of the external load (Watkins 2004). Wilson (2011) invented a medium-duty bridge structure that incorporates corrugated metal plate and concrete in a manner that forms a composite load-bearing structure. This structure comprises at least one corrugated metal plate with corrugations oriented parallel to the longitudinal axis of the bridge structure. A layer of concrete is applied to the upper surface of this corrugated metal plate to provide a support surface. Machelski and Tomala (2012) presented analyses of the efficiency of additional ribs filled with concrete in single-corrugated overlapped plates. The findings of these analyses may allow the estimation of both shell displacement during backfilling and internal forces under live loads. The paper also demonstrated that the connection stiffness depends on the load intensity in the operational range. Kang and Davidson (2013) evaluated the soil-structure interactions of CLCSPs and compared them with those of unlined CSPs. The results showed that the use of a concrete lining for CSPs reduced the maximum stresses within the CSPs significantly. The highest tensile stresses in the concrete lining were induced at the crown. The governing design factor for CLCSPs is the tensile strength of the concrete, rather than deflection. From the above, the composite structure of corrugated steel plate and concrete has application prospects in engineering practice due to its enhanced strength, stiffness and stability.

However, previous studies concentrated only on corrugated steel and normal concrete. Several studies have been devoted to the possibility of using rubber recovered from scrap tires to replace natural aggregates in concrete because of the static and dynamic performance of this material. Atahan and Yücel (2012) verified that increasing the fraction of rubber particles decreased the compressive strength and elastic modulus of concrete while significantly increasing impact time and energy dissipation capacity. Aiello and Leuzzi (2010) showed the rubberized concrete mixtures had lower unit weight compared to plain concrete and better working ability. The results of compression and bending tests indicated a larger reduction of mechanical properties of rubberized concrete when replacing coarse aggregate rather than fine aggregate. Rubberized concrete showed good energy absorption and ductility in the range observed for fibrous concrete, as suggested by standard ASTM C1018-97 (1997). Gupta et al. (2014) proved that flexural strength of rubber ash concrete decreased with increased rubber ash percentage, whereas flexural strength of modified concrete increased with increased rubber fiber percentage. The abrasion resistance, carbonation depth, modulus of elasticity and chloride-ion penetration of rubber ash concrete and modified concrete were also affected by the addition of rubber ash and rubber fibers. Those studies show that rubberized concrete, an eco-friendly and waste-based material, has improved impact resistance and energy dissipation capacity compared with normal concrete but decreased strength and modulus of elasticity. In this paper, the composite structure properties of rubberized concrete are studied and compared with those of normal concrete.

To study the mechanical and composite performance of the CSP-concrete structure with normal and rubberized concrete, one CSP-normal-concrete plate and two CSP arches composited with different concretes (normal and rubberized), were established. Theoretical deduction and finite element calculation were conducted to compare the experiments. The testing results verified the effectiveness of theoretical deduction and numerical models.

Additionally, the stress of the concrete and steel in critical measuring points (MPs) on the plate and arches were obtained using the loading test. Deflections were measured to reflect the features of flexural rigidity and compressive stiffness. Moreover, natural frequency and damping ratio were obtained to investigate dynamic characteristics.

2 Deduction of Composite Property

2.1 Theoretical Deduction

Corrugated steel plate-concrete composite structure is composed of concrete on the top and CSP on the bottom connected via welding steel beams or long bolts (Fig. 1). In the elastic stage, the calculation of cross-sectional properties can be done using two methods. The first involves getting the equivalent flexural and compressive modulus according to the principle of unchanged flexural and compressive stiffness (Wen 2012). The second, which was used in this paper, involves converting the section into steel materials. Take this section, for example, where Es represents the actual steel material. The total I' (moment of inertia) and A' (area) should be converted to pure steel.

The difficulty is shaping the concrete part when changing it into an equivalent steel section. Therefore, three assumptions are given as follows:

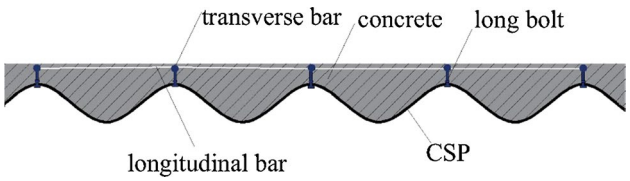

Fig. 1 Schematic diagram of CSP-concrete composite structure model

(1) Both steel and concrete have the same contact surface strain (fiber deflection consistency).
(2) The total section has the same resultant when transformed into pure steel.
(3) The current and transformed sections have the same centroid position.

Assuming α_e is the modulus ratio of steel to concrete, (1) regard CSP's line shape as a cosine curve; and (2) the primary concrete area is A_c, and the equivalent steel area is A_c'. Select a wavelength for the CSP-concrete composite structure and schematic diagram as shown in Fig. 2.

Calculation of the composite properties can be acquired as follows:

$$\frac{E_s}{E_c} = \frac{\sigma_s}{\sigma_c} = \alpha_e \tag{1}$$

$$y_1(x) = \frac{h}{2}\cos\left(\frac{2\pi}{b}\left(x + \frac{b}{2}\right)\right) + \frac{h}{2} \tag{2}$$

$$y_2(x) = \frac{h}{2}\cos\left(\frac{2\pi\alpha_e}{b}x + \pi\right) + \frac{h}{2} \tag{3}$$

$$b_{eq} = \frac{b}{\alpha_e} \tag{4}$$

where E_s, modulus of steel; E_c, modulus of concrete; α_e, ratio of E_s to E_c.

The centroid of the concrete y_c can be calculated using Eq. (5). Then the centroid of the composite section y_{cp} is calculated by using Eq. (6).

$$y_c = \frac{\int_{A_c} y dA_c}{\int_{A_c} dA_c} \tag{5}$$

$$y_{cp} = \frac{A_s\frac{h}{2} + \frac{A_c}{\alpha_e}y_c}{A_s + \frac{A_c}{\alpha_e}} \tag{6}$$

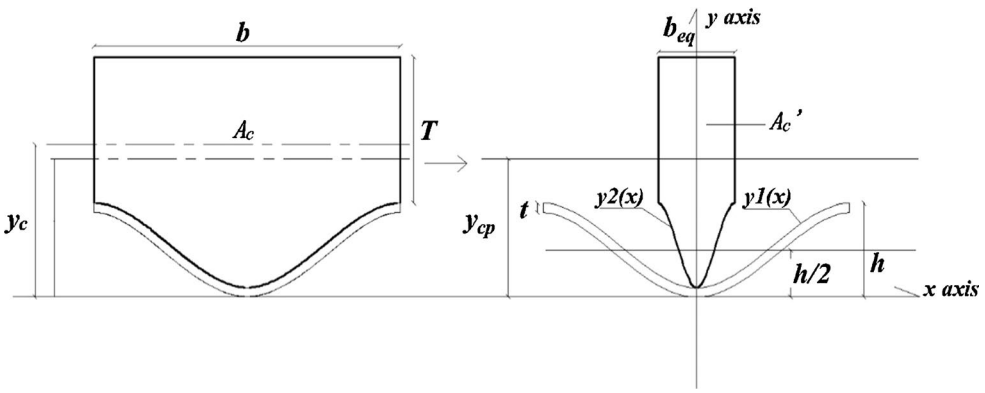

Fig. 2 Schematic diagram of composite property calculation. Here $y_1(x)$ and $y_2(x)$, are the shape function of CSP; b, wave pitch of the CSP; b_{eq}, length of equivalent steel materials transformed by former concrete; T, width of concrete covering; t, plate thickness of CSP; h, wave depth of CSP; y_c, the centroid of the concrete; y_{cp}, the centroid of the composite section

Therefore, the moment of inertia I' and area A' of the composite cross-section can be calculated as follows:

$$I' = I_s + A_s\left(y_{cp} - \frac{h}{2}\right)^2 + \int_{A_c'} y^2 dA_c' - \frac{A_c}{\alpha_e} y_c^2 + \frac{A_c}{\alpha_e}(y_{cp} - y_c)^2$$
$$= I_s + A_s\left(y_{cp} - \frac{h}{2}\right)^2 + \int_{A_c'} y^2 dA_c' - \frac{A_c}{\alpha_e} y_c^2 + \frac{A_c}{\alpha_e} y_{cp}(y_{cp} - 2y_c) \quad (7)$$

$$A' = A_s + \frac{A_c}{\alpha_e} \quad (8)$$

In Eqs. (7)–(8), concrete material is converted to steel. Here A_s, area of steel; A_c, area of sectional concrete; I_s, CSP's moment of inertia (Feng 2006).

2.2 Theoretical Stress and Deflection Calculation

One composite plate and two composite arches have been established. Material parameters are presented in Table 1. Cross-sections of the plate and arches are shown in Fig. 3.

The method in Sect. 2.1 can be applied using manual calculation or Math CAD expressions to calculate the properties of the composite section with different materials. One baseline material must be chosen firstly, then by changing other materials into the baseline material, the composite section can be converted to a single material section using the method discussed in Sect. 2.1. The calculation results are given in Tables 2 and 3.

It can be observed that the compressive stiffness and flexural rigidity of the CSP-concrete composite structure are significantly higher than those of the CSP structure. This finding can be attributed to the stiffness redistribution that disperses the force onto the steel and concrete. The compressive stiffness and flexural rigidity of

Table 1 Material parameters of the models

	Normal concrete 1	Normal concrete 2	Rubberized concrete
Elastic modulus (Pa)	2.50E+10	1.79E+10	1.31E+10
Compressive strength (MPa)	16.7	16.6	12.2
Application	Normal concrete composite arch	Normal concrete composite plate	Rubberized concrete composite arch

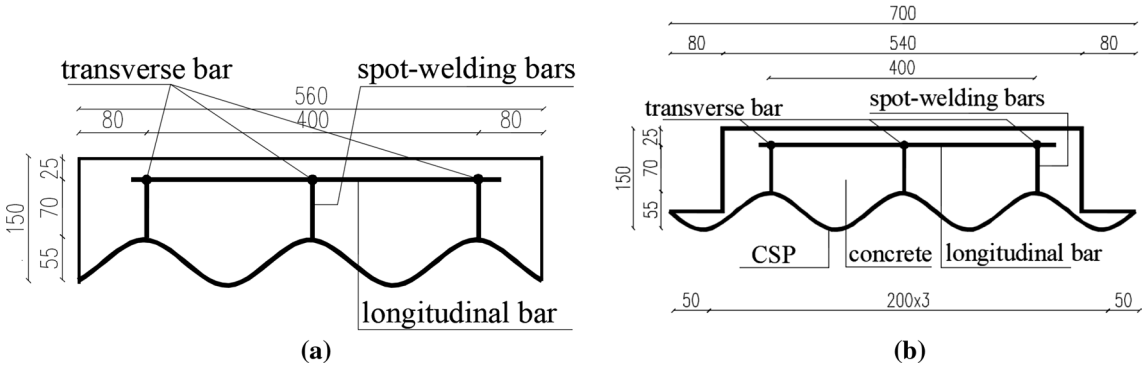

Fig. 3 Cross-sections of members. **a** Cross-section of plate (mm). **b** Cross-section of arches (mm)

Table 2 Flexural rigidity and compressive stiffness of the composite plate

	CSP	Concrete	Composite structure	Times
Area (mm^2)	3754	70,787	9905	2.64
Compressive stiffness (N)	773,324	1,267,100	2,040,508	2.64
Moment of inertia (mm^4)	1,208,215	106,808,988	20,485,953	16.9
Flexural rigidity (N m^2)	248,892	1,911,881	4,220,106	16.9
y (mm)	29	–	89.5	–
y′ (mm)	31.7	–	72.3	–

Table 3 Flexural rigidity and compressive stiffness of the composite arches

	CSP	Normal concrete composite			Rubberized concrete composite		
		Concrete	Composite structure	Times	Concrete	Composite structure	Times
Area (mm^2)	4740	66,110	12,763	2.69	66,110	8945	1.89
Compressive stiffness (N)	976,440	1,652,750	2,629,255	2.69	866,041	1,842,670	1.89
Moment of inertia (mm^4)	1,581,566	93,768,308	26,724,135	16.9	93,768,308	17,835,508	11.2
Flexural rigidity (N m^2)	325,803	2,344,208	5,505,172	16.9	1,228,365	3,674,115	11.2
y (mm)	33	–	87.8	–	–	91.5	–
y′ (mm)	27.6	–	70.4	–	–	70.1	–

the rubberized concrete composite arches are lower than those of normal concrete composite arches.

Based on the results in Tables 2 and 3, in mid-span section of normal concrete composite plate and arches, vertical deflection δ and steel normal stress σ_{spt} on the valley of the CSP plate can be calculated as follows:

$$\delta = \int \frac{MM'}{E_s I'} ds \tag{9}$$

$$\sigma_{spt} = \frac{My'}{I'} \tag{10}$$

where M, bending moment under external load; M', bending moment of micro-segment ds under unit load; $E_s I'$, the flexural rigidity; y', the distance between the centroid and the corrugation valley; y, the distance between the centroid and top of concrete.

The calculation results are presented in Tables 2 and 3.

Additionally, concrete stress σ_{cpt} on the top position of concrete in the mid-span position can be obtained using Eq. (1) and Eqs. (11)–(12):

$$\alpha_{el} = \frac{E_s}{E_{cpt}} \tag{11}$$

$$\sigma_{cpt} = \frac{\sigma_{spt}}{\alpha_{el}} = -\frac{My}{I'} \frac{1}{\alpha_{e1}} \tag{12}$$

where α_{el}, ratio between modulus of steel and normal concrete; E_{cpt}, modulus of normal concrete.

The method in Sect. 2.1 has presented a simplification to calculate a composite cross-section that can be used to calculate the sectional properties of the CSP-concrete composite. With the sectional properties obtained in Tables 2 and 3, the stress and deflection of the structure can be calculated theoretically. The results of stress and deflection on the mid-span of normal concrete composite structures are given in Table 4.

Table 4 Stresses and deflection results in the mid-span (Normal concrete)

Type	Plate	Arch
Stress on CSP valley (steel) (MPa)	19.99	4.15
Stress on concrete top (MPa)	−2.15	−0.75
Deflection (mm)	−0.492	0.25

Fig. 4 CSP-concrete plate model

3 Model Test

3.1 Plate Test

The plate, having a span of 2.1 m, was simply supported as shown in Fig. 4.

The plate was loaded by two-point concentrated weight loads implemented by a distribution beam and two cylindrical steel rods as shown in Fig. 5. The load process has four stages as shown in Table 5.

The vertical deflection was tested using micrometers. The stress of corrugated steel plate and concrete was tested using steel strain gauges and concrete strain gauges, respectively. Strain results were collected using a programmable static resistance strain gauge.

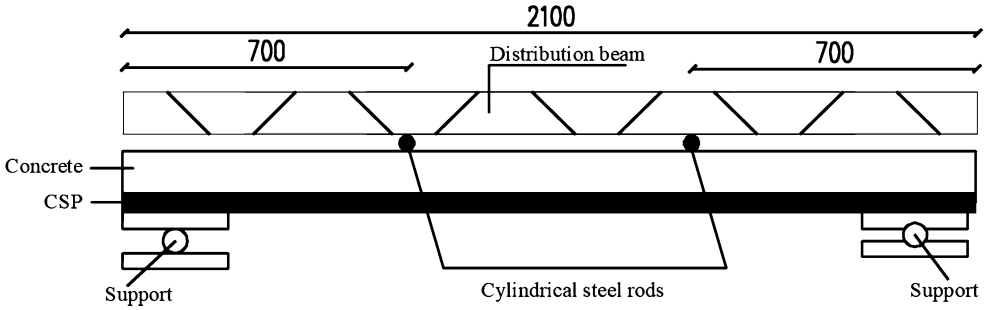

Fig. 5 Loading on plate model (mm)

Table 5 Hierarchical loading on plate

Loading stage	Mass (kg)	Aggregation (kg)
1	546	546
2	515	1061
3	515	1576
4	515	2091

Fig. 6 CSP-concrete arch model

3.2 Arch Test

The boundary conditions of the arches were hinge joint on both sides of arch springing. The span and rise of the arches were 3.44 m and 1.69 m. Three lateral ties welded onto the arch springing were used to offset lateral thrust as shown in Fig. 6.

The test instruments and methods of arches were similar as plate. Two-point concentrated loads were added on the symmetric position on the crown by using a simple distribution girder as shown in Fig. 7. The load process included four stages as shown in Table 6.

To investigate the dynamic properties of the two arches, natural frequency and damping ratio were measured using a multipoint hammering system using the hammer excitation with Single Input and Multiple Output (SIMO) method (Fig. 8).

3.3 Measuring Point (MP) Arrangement

For CSP-concrete plate, control sections were chosen in three critical sections: mid-span and two loading sections. Three vertical deflection MPs (D1–D3), six CSP steel stress MPs (S1–S6), and five concrete stress MPs (C1–C5) were arranged. Steel gauges were placed on the inside surface of the CSP at wave valleys (S1, S2, S5) and crests (S3, S4, S6) as shown in Fig. 9.

For arches, the MP arrangement is shown in Fig. 10.

The arrangement of the MPs was roughly the same as that of the plate, except that the shoulders (30° from horizon) and mid-span of arches had three critical sections.

4 Test Results Analysis

4.1 Displacement

4.1.1 Plates

The displacement results of normal concrete composite plates are shown in Fig. 11.

According to Fig. 11, displacement increases by 0.2 mm with each loading stage and the load–deflection curve is largely linear, indicating the structures are within the elastic state. In general, the displacement of D1 and D2 in normal concrete composite plate is nearly the same, and that of D3 is a little higher. Deflection at D1, D2 and D3 is 0.598 mm, 0.798 mm and 0.662 mm, respectively.

4.1.2 Arches

The displacement results of normal and rubberized concrete composite arches are shown in Fig. 12. A positive value indicates that the position is concave and a negative value indicates the position is convex.

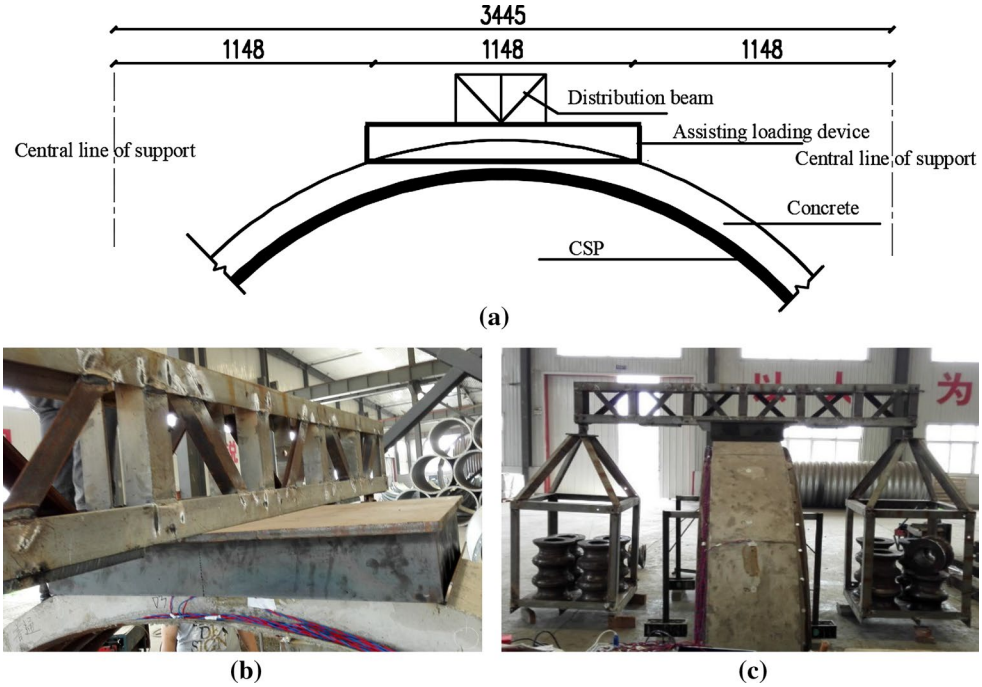

Fig. 7 Loading on arch model. **a** Loading on arch model (mm). **b** Loading devices. **c** The 4th grade loading (2 tons)

Table 6 Hierarchical loading on arches

Loading stage	Mass (kg)	Aggregation (kg)
1	480	480
2	502	982
3	502	1484
4	544	2028

Fig. 8 Dynamic characteristics test

It can be seen from Fig. 12 that the shoulders of the two arches (D1, D2) are convex and the crowns (D3) are concave. Because the side of D1 is near the fixed-hinge support and the side of D2 is near the rolling support, the simply supported system extends in the axial direction of the transverse pull rods, which results in the radial deflection of D2 being greater than that of D1. After loading, the deflection of the normal concrete arch at D1, D2 and D3 is −0.074 mm, −0.414 mm and 0.321 mm, respectively, while that of the rubberized concrete plate is −0.126 mm, −0.628 mm and 0.634 mm, respectively.

In general, the radial deflection of the rubberized concrete composite arch is larger than that of the normal one because rubber particles reduce the elastic modulus of rubberized concrete and result in a decrease in compressive and bending stiffnesses. With the arch ring as the bending component, the redistribution of stiffness causes a larger deformation in the rubberized concrete composite arch.

4.2 Stress

In the figures below, negative stress values indicate the positions are compressed and positive values indicate the positions are in tension.

4.2.1 Plate

The stress results of normal concrete composite plate are shown in Fig. 13.

According to Fig. 13, the stress of wave valleys (S1, S2) and wave crests (S3, S4) at loading sections changes consistently and the stress of wave valleys is greater than the stress of wave crests. In the mid-span section, the stresses of the wave valley (S5) and wave crest (S6) are slightly less than those of loading sections. All of the MPs of the steel plate are in tension. After loading, the stresses of the wave valleys (S1, S2) at loading sections are 22.4 MPa and 21.2

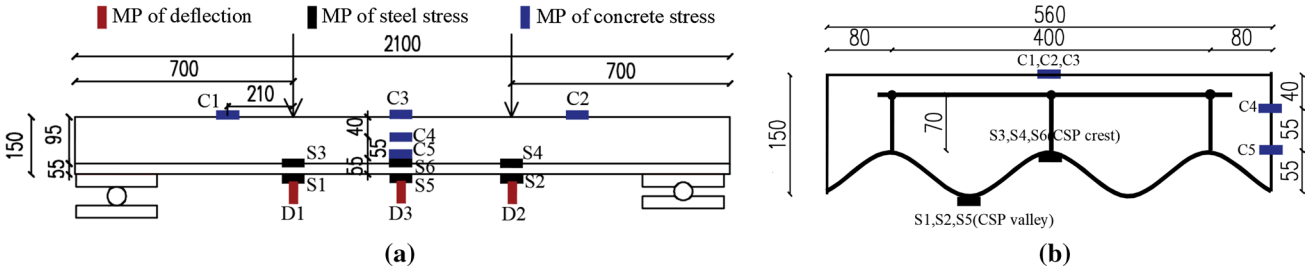

Fig. 9 Measuring point (MP) arrangement of the plate (mm). **a** Vertical section. **b** Cross-section

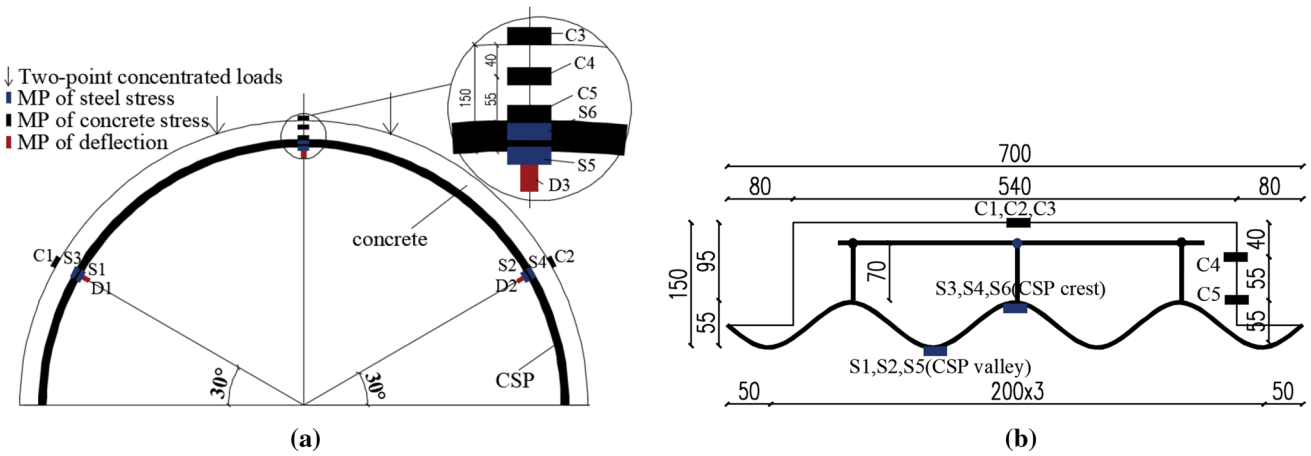

Fig. 10 Measuring point (MP) arrangement of the arches (mm). **a** Vertical section. **b** Cross-section

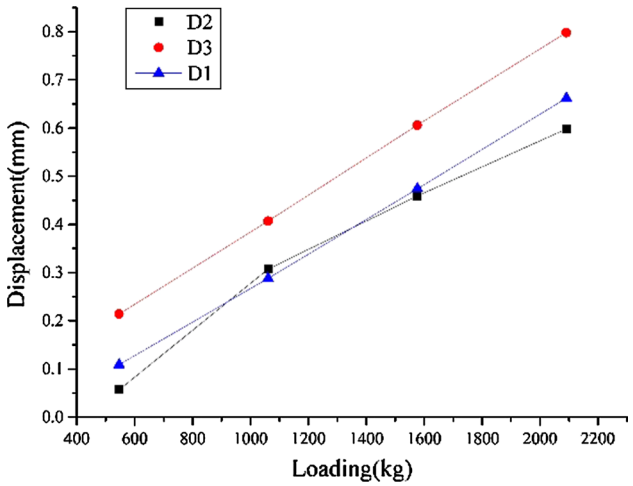

Fig. 11 Displacement of MPs on a normal composite plate

MPa, respectively, and those of the wave crests (S3, S4) are 7.2 MPa and 7.8 MPa, respectively. In the mid-span section, the stresses of the wave valley (S5) and wave crest (S6) are 19.2 MPa, 2.7 MPa, respectively.

The stress of concrete at the top (points C1–C3) of the plate are all negative which means those points are compressive. In the mid-span section, the compressive stress of top point C3 is the largest and the following is compressive stress of the point C4. While C5 shows a small tensile stress, which may be due to the position of it is at the neutral axis. After loading, concrete stress at the top of plate (C1 and C2) is 1.43 MPa, 1.16 MPa. In the mid-span section, the concrete stress value from top to bottom (C3–C5) is 4.99 MPa, 1.95 MPa, 0.16 MPa.

Combining the results of steel and concrete, the bottom of the structure is in tension and the upper concrete is compressive. The concrete compressive stress of the pure bending segment in the mid-span section decreases from top to bottom, while the tensile stress in the steel plate decreases from bottom to top.

4.2.2 Arch

The stress results of the normal concrete composite arch are shown in Fig. 14.

According to Fig. 14, the stress-load curve is basically linear, which means the structure is within the elastic state. The tangential stress of wave valleys (S1, S2) is greater than that of wave crests (S3, S4) at the shoulders, because the inner ring is compressed and outer ring is in tension in the

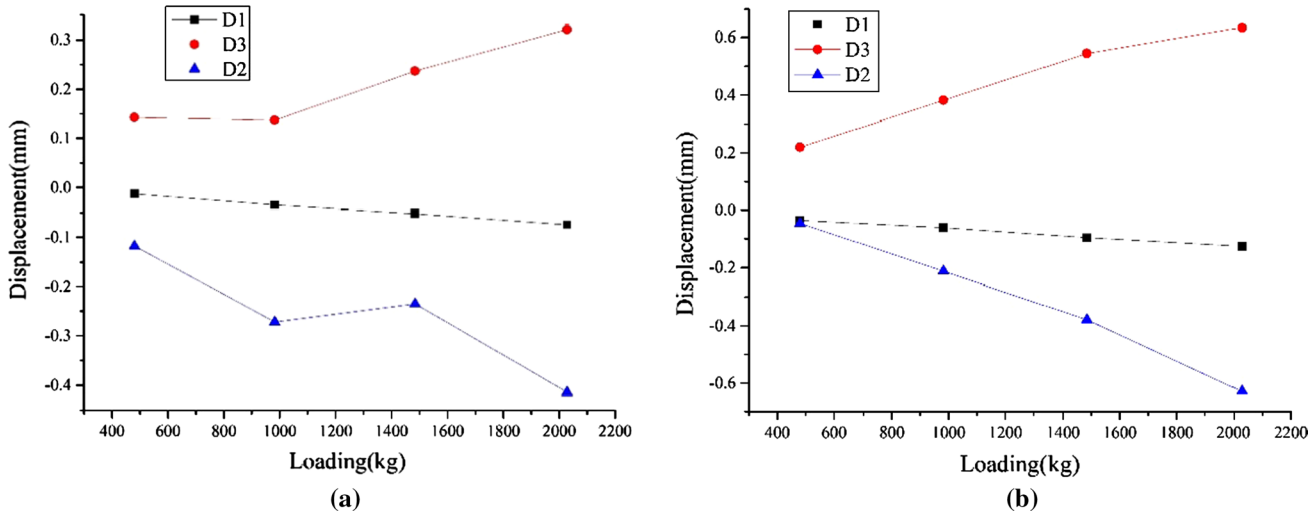

Fig. 12 Displacement of MPs on composite arches. **a** Normal concrete composite arch. **b** Rubberized concrete composite arch

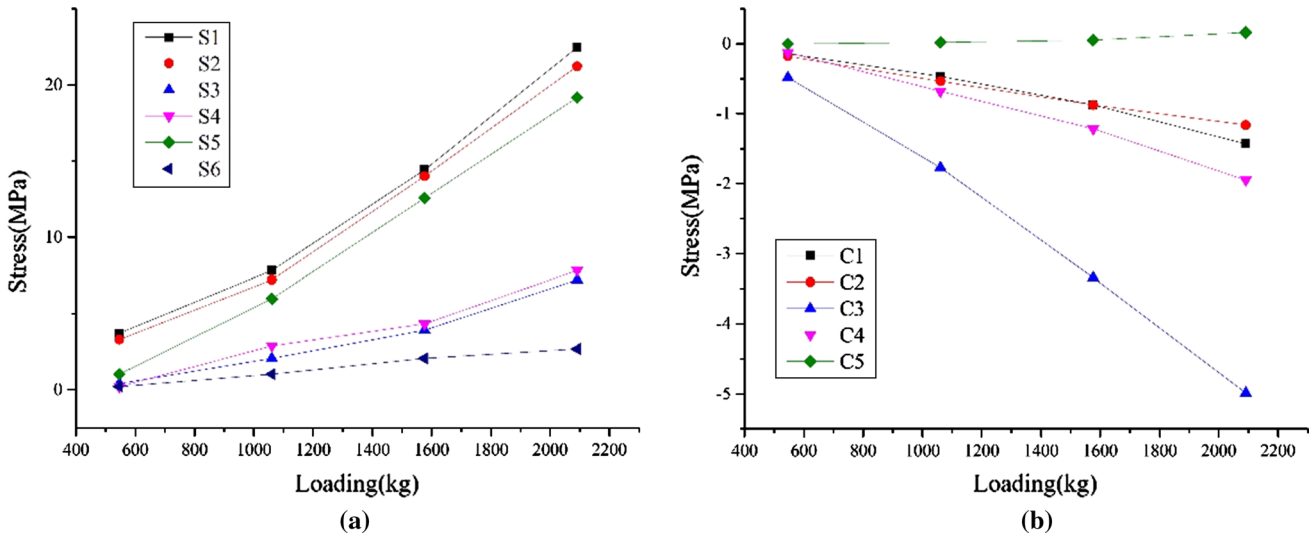

Fig. 13 Stress of MPs on normal concrete composite plate. *All the steel and concrete stresses of the plate models are the normal stress along the plate. **a** Stress of steel. **b** Stress of concrete

negative moment region. However, there is an axial force that can offset the tensile stress in the inner ring and compress the wave crests and valleys. In the mid-span section, the stresses of the wave valley (S5) and crest (S6) are lower than the corresponding positions of the arch shoulders. After loading, the stresses of the wave valleys at the shoulders (S1, S2) are − 10.9 MPa and − 10.5 MPa, respectively, and those of wave crests (S3, S4) are − 6.0 MPa and − 6.4 MPa, respectively. In the mid-span section, the stresses of the wave valley (S5) and wave crest (S6) are 2.47 MPa and − 2.47 MPa, respectively.

The concrete MPs (C1–C2) at the outer shoulders are all positive which means those points are in tension, as those positions are in the negative moment region. In the mid-span section, the compressive stress of point C3 is the largest, followed by the compressive stress of point C4. Point C5 has a small tensile stress, which may be because it is at the neutral axis. After loading, the concrete stresses at the shoulders (C1 and C2) are 1.18 MPa and 1.45 MPa, respectively. In the mid-span section, the concrete stresses of the points from top to bottom (C3–C5) are − 0.7 MPa, − 0.28 MPa and − 0.25 MPa, respectively.

The stress results of the rubberized concrete composite plate are shown in Fig. 15.

According to Fig. 15, the stress trends of the rubberized concrete composite arch are consistent with that of the

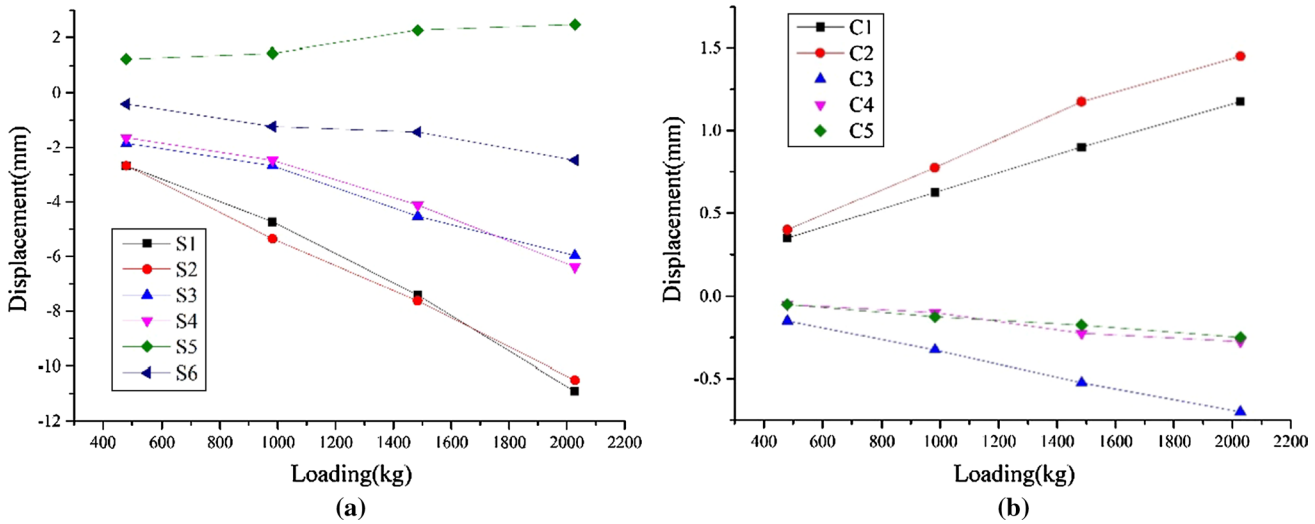

Fig. 14 Stress of MPs on the normal concrete composite arch. *All the steel and concrete stress of the arch models is circular normal stress along the arch ring. **a** Stress of steel. **b** Stress of concrete

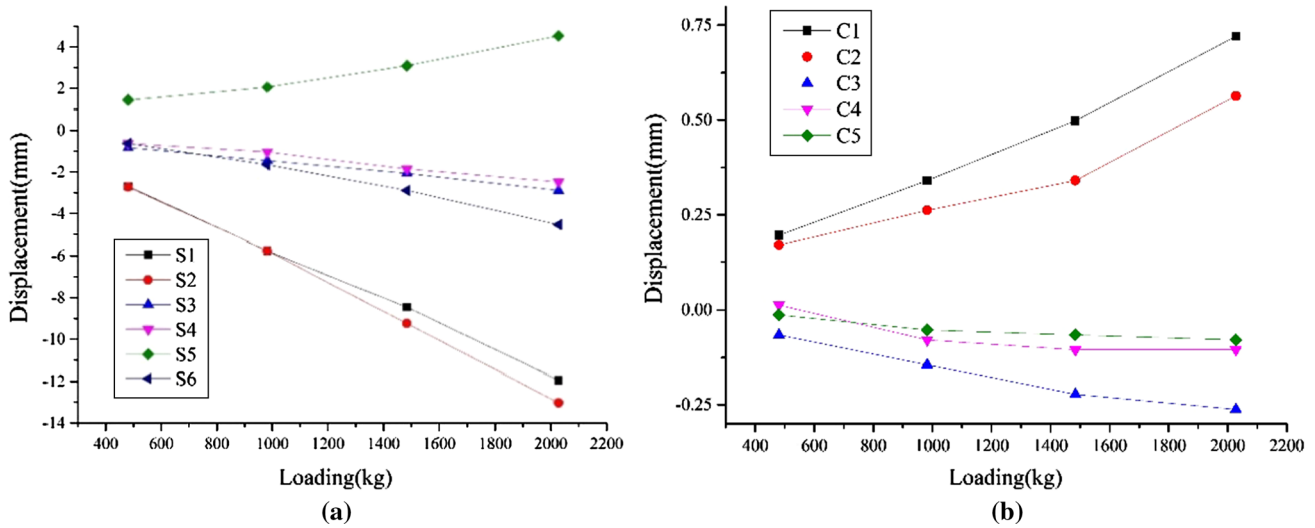

Fig. 15 Stress of MPs on rubberized concrete composite arch. **a** Stress of steel. **b** Stress of concrete

normal concrete composite arch. After loading, the stresses of the rubberized concrete composite at the wave valleys (S1, S2) of the shoulder sections are − 12.0 MPa and − 13.0 MPa, respectively, and those at the wave crests (S3, S4) are − 2.9 MPa and − 2.5 MPa, respectively. In the mid-span section, the stresses at the wave valley (S5) and wave crest (S6) are 4.5 MPa and − 4.5 MPa, respectively. The concrete stresses at the shoulders (C1 and C2) are 0.72 MPa and 0.56 MPa, respectively. In the mid-span section, the concrete stresses from top to bottom (C3–C5) are − 0.26 MPa, − 0.1 MPa and − 0.08 MPa, respectively.

In general, the steel stress at the wave valleys of the shoulder sections in the rubberized concrete composite arch is greater than that in the normal concrete composite arch. In the mid-span section, the steel stress of the rubberized concrete composite arch is greater than that of the normal concrete composite arch. This property is due to a decrease

Table 7 Summary of dynamic characteristics

Models	Natural frequency (Hz)	Damping ratio (%)
Normal concrete composite plate	64.151	3.75
Normal concrete composite arch	16.868	9.22
Rubberized concrete composite arch	14.763	11.56

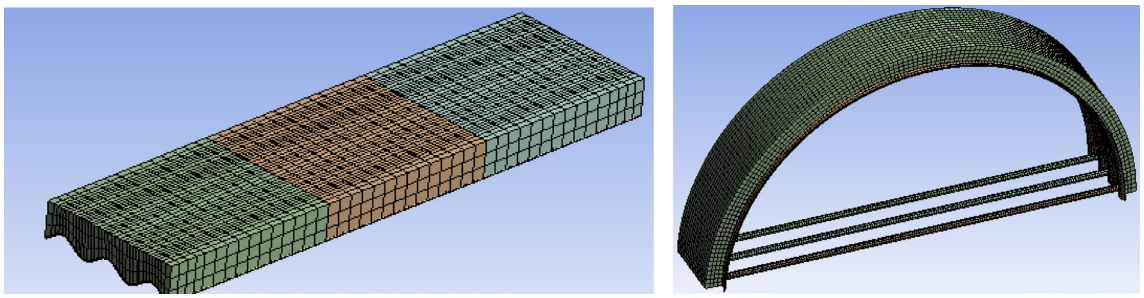

Fig. 16 Finite element models of concrete composite plate and arch

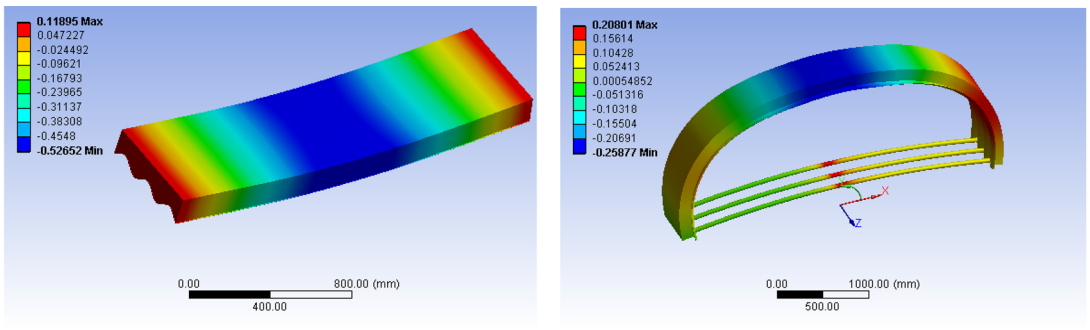

(a)

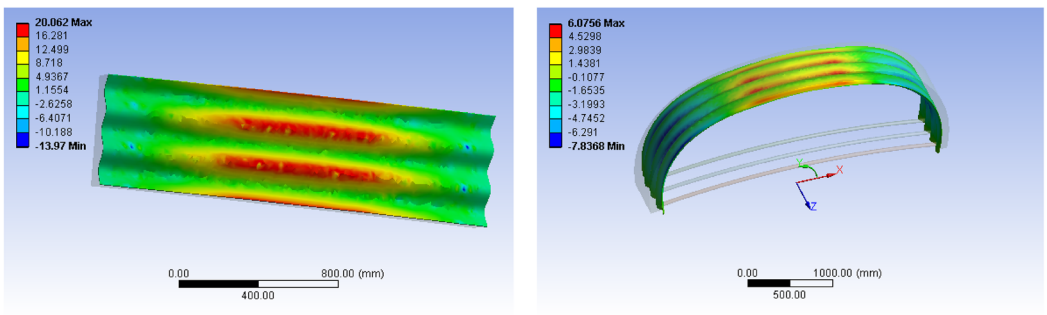

(b)

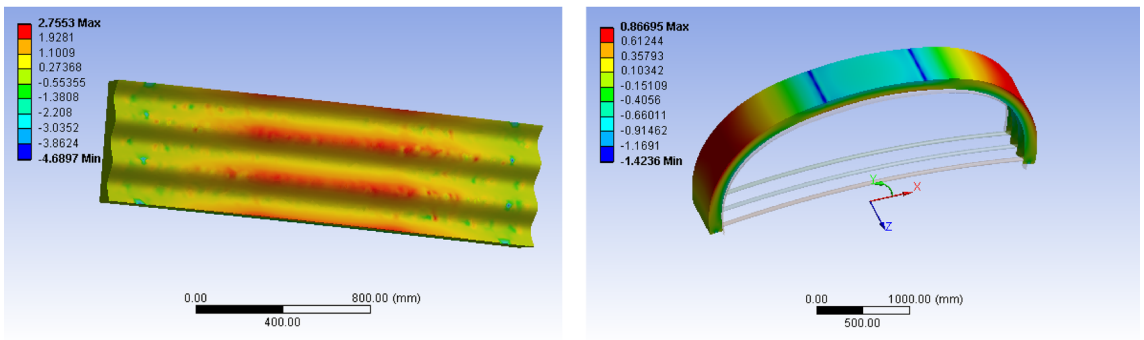

(c)

Fig. 17 Numerical results of normal concrete plate. **a** Vertical deflection (steel and concrete) (mm). **b** Normal stress of steel (MPa). **c** Normal stress of concrete (MPa)

Table 8 Comparison of experimental, numerical and theoretical results of the plate

	Deflection (mm)	Normal stress of steel (MPa)				Normal stress of concrete (MPa)		
Experimental results	−0.798	Corrugation crests	S1	S2	S5	C3	C4	C5
			22.4	21.2	19.2			
		Corrugation valleys	S3	S4	S6	−4.99	−2	0.2
			7.2	7.8	2.7			
FE method results	−0.527	Corrugation crests	S1, S2, S5			C3	C4	C5
			20.6					
		Corrugation valleys	S3, S4, S6			−2.16	−1	0.3
			4.9					
Theoretical calculation	−0.746	Corrugation crests	S1, S2, S5			C3	C4	C5
			19.99					
		Corrugation valleys	S3, S4, S6			−2.15	−1	0.1
			4.78					

in elastic modulus of rubberized concrete, which leads to a decrease in flexural and compressive stiffnesses.

4.3 Dynamic Characters

The results of the dynamic tests are summarized as shown in Table 7.

According to Table 7, the first frequency of the rubberized concrete composite arch is lower than that of the normal concrete composite arch and the damping ratio is larger, which means the dynamic performance and energy dissipation effects of rubberized concrete structures are better than those of normal concrete structures. That is, rubberized concrete is better in projects demanding energy dissipation, but not those demanding strength and stiffness.

5 Finite Element Numerical Analysis

Finite element models with normal concrete were built to be compared with the experimental results shown in Fig. 16.

With the numerical simulation in the FE platform, the deflection of model as well as normal stress of steel and concrete is presented in Fig. 17. And the comparison between measured, numerical and theoretical results is shown in Tables 8 and 9.

As is shown in Tables 8 and 9, the steel stress of the theoretical calculation and finite element analysis are basically the same, especially at the wave crests. The theoretical deflection is close to that of the experimental results, but

Table 9 Comparison of experimental, numerical and theoretical results of the arch

Deflection (mm)		Normal stress of steel (MPa)				Normal stress of concrete (MPa)		
Experimental results								
D1	−0.074	Corrugation crests	S1	S2	S5	C1	C2	C3
D2	−0.414		−11	−11	2.5			
D3	0.321	Corrugation valleys	S3	S4	S6	1.2	1.5	−0.7
			−6	−6	−2			
FE model results								
D1	−0.11	Corrugation crests	S1, S2		S5	C1, C2		C3
D2	−0.19		−7.41		4.1			
D3	−7.41	Corrugation valleys	S3, S4		S6	0.79		−0.3
			−2.57		0.6			
Theoretical calculation								
D3	0.25	Corrugation crests	S5			C3		
			4.15					
		Corrugation valleys	S6			−0.75		
			0.54					

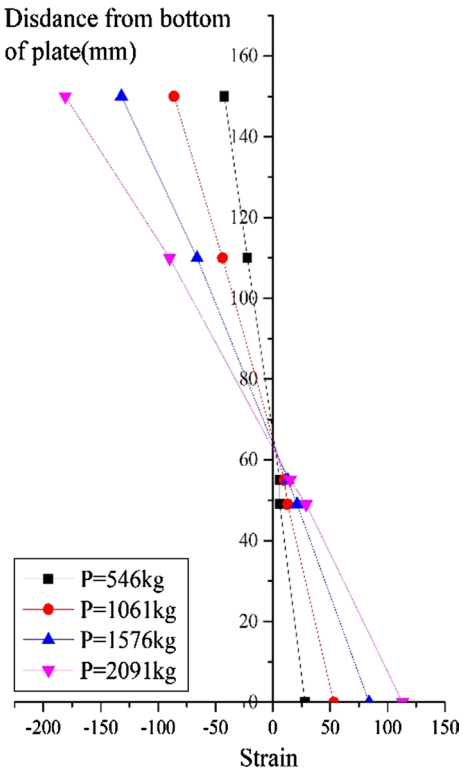

Fig. 18 Plane section strain in mid-span under each loading

there were slight differences when the finite element results were compared with the experimental results.

The concrete stress of the theoretical calculation and that of the FE analysis are remarkably close for the composite plate, while those of the experimental results is slightly more divergent. In the composite arch, the concrete stress of the experimental results is closer to that of the theoretical calculation than the FE results.

Interfacial slippage of steel and concrete in the experiment caused differences in the neutral axis location between the experimental and finite element models. Therefore, comparisons can only be made qualitatively.

6 Composite Characters Analysis

The plane section strain in the mid-span of the normal concrete plate of the four stages of loading as shown in Fig. 18.

According to Fig. 18, the longitudinal strain distribution along the depth of the cross-section obeys the plain-section strain assumption. This finding implies that the CSP-concrete composite plate exhibits a preferable combined performance. The strain of the FE plate model in mid-span position is shown in Fig. 19.

Due to the ideal combination at the interface, strain spreads continuously and tensile stress decreases gradually from bottom to top and is 0 at the neutral axis. Then, the compressive strain appeared and increased to a maximum at the top of the concrete. This shows that bounding contacts can make models meet the plane-section assumption better. Moreover, the neutral axis position and concrete cracking area can be addressed, which provides a reference for the optimization and design of composite structures in the future.

7 Discussion and Conclusions

- A simplified theoretical deduction for such CSP-concrete composite section properties calculation was introduced and results on theoretical calculation indicated that flexural and compressive stiffness had improved after combination. In particular, the flexural stiffness of CSP-Concrete composite structure notably increased when compared with traditional CSP structure.
- After comparing the results of the experimental, numerical and theoretical results, the effectiveness of theoretical and numerical solutions was verified. Nevertheless, interfacial slippage of steel and concrete in the experiments caused differences in the neutral axis location between experimental and FE models without considering interfacial slippage. An elaborate FE model is more suitable for such a composite structure.
- The rubberized concrete composite arch has lower flexural rigidity and compressive stiffness, resulting in larger deflection compared with the normal concrete composite arch. The smaller stiffness of the rubberized concretes caused stress redistribution in the rubberized concrete

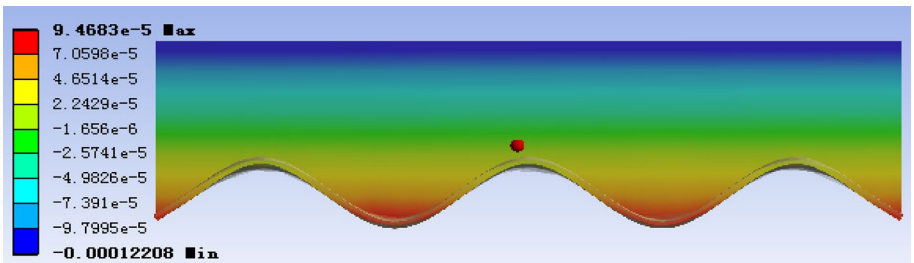

Fig. 19 Strain in the mid-span position of the normal concrete composite plate

composite arch compared with the normal concrete composite arch. The rubberized concrete composite arch has higher steel stress and lower concrete stress compared with the normal one.

- Owing to the larger damping ratio of the rubberized concrete composite structure, the energy-dissipating capacity of rubberized concrete composite structures is better than that of normal ones. Therefore, the structure of the CSP-rubberized concrete composite is more suitable for anti-shock and earthquake-resistant structures.
- The strain in the elastic stage of the CSP-concrete composite plate was confirmed to meet the plane-section assumption through analysis of the measured strain in the mid-span of the plate section. The neutral axis position and concrete cracking area warrant further research to provide a reference for the optimization and design of composite structures in the future.

Acknowledgements This work was supported by the National Natural Science Foundation of China (51478030). The authors of this paper would like to warmly thank the Hebei Tengshida Metal Structure Corporation for their assistance during experimental testing.

References

Aiello, M. A., & Leuzzi, F. (2010). Waste tyre rubberized concrete: properties at fresh and hardened state. *Waste Management, 30*(8–9), 1696.

ASTM C1018-97 (1997). Standard test methods for flexural toughness and first crack strength of fibre reinforced concrete. *American Society for Testing and Materials (ASTM), 4*(2), 506–513.

Atahan, A. O., & Yücel, A. Ö. (2012). Crumb rubber in concrete: Static and dynamic evaluation. *Construction and Building Materials, 36*(4), 617–622.

Beben, D. (2014). Corrugated steel plate culvert response to service train loads. *Journal of Performance of Constructed Facilities, 28*(2), 376–390.

Choi, D.-H., Na, H.-S., & Kim, G.-N. (2009). Modification of moment equations in the CHBDC (2000) for soil-metal box structures. *International Journal of Steel Structures, 9*(4), 343–354.

Feng, Z. (2006). *Analysis and design method study on soil-steel interaction in buried corrugated steel bridge*. Master-degree Dissertations, Beijing Jiaotong University, Beijing. **(in Chinese)**.

Flener, E. B. (2009). Response of long-span box type soil-steel composite structures during ultimate loading tests. *Journal of Bridge Engineering, 14*(6), 496–506.

Gupta, T., Chaudhary, S., & Sharma, R. K. (2014). Assessment of mechanical and durability properties of concrete containing waste rubber tire as fine aggregate. *Construction and Building Materials, 73*(73), 562–574.

Kang, J. S., & Davidson, J. S. (2013). Structural effects of concrete lining for concrete-lined corrugated steel pipes. *Structure & Infrastructure Engineering, 9*(2), 130–140.

Liu, Q. (2001). Experimental results and preliminary analysis on three-dimensional CSP concrete-lining. In *National modern structural engineering academic meeting*, Tianjin, China. **(in Chinese)**.

Machelski, C., Michalski, J. B., & Janusz, L. (2013). Parametric analysis of corrugated steel plate structures with maximum spans. In *Transportation research board 92nd annual meeting*.

Machelski, C., & Tomala, P. (2012). Stiffness of shells with concrete filled ribs in soil-steel bridge structures. *Archiwum Instytutu Inżynierii Lądowej, 12,* 157–166.

Morrison, T. D. (2005). Innovative low cover bridges utilizing deep-corrugated steel plate with encased concrete composite ribs. In *2005 annual conference of the transportation association of Canada*.

Vinoth Kumar, K., & Kavitha, A. (2016). Experimental study on composite sandwich panels with concrete and corrugated steel faces. *International Journal for Scientific Research & Development, 4*(01), 939–942.

Watkins, R. K. (2004). Buried pipe encased in concrete. In *Pipeline division specialty congress* (pp. 1–10).

Wen, J. (2012). Back analysis for the mechanical properties of initial tunnel support based on steel arch stresses. *China Civil Engineering Journal, 45*(2), 170–175. **(in Chinese)**.

Wilson, M. W. (2011). *Corrugated metal plate bridge with composite concrete structure*. US, US7861346.

Yu, H., Tan, N., & Chen, X. (2012). Calculation method of reinforced concrete shell with CSP lining. *Jiangsu Construction, 148,* 75–78. **(in Chinese)**.